Multiple-Exposure PTV With Variable Time Steps

Scarano, F.; Hysa, I.; Grille Guerra, A.; Tuinstra, Marthijn; Sciacchitano, A.

DOI
10.55037/lxlaser.21st.151

Publication date
2024

Document Version
Final published version

Published in
Proceedings of the 21st International Symposium on the Application of Laser and Imaging Techniques to Fluid Mechanics

Citation (APA)
Scarano, F., Hysa, I., Grille Guerra, A., Tuinstra, M., & Sciacchitano, A. (2024). Multiple-Exposure PTV With Variable Time Steps. In *Proceedings of the 21st International Symposium on the Application of Laser and Imaging Techniques to Fluid Mechanics* Article 151 LISBON Simposia. https://doi.org/10.55037/lxlaser.21st.151

Multiple-exposure PTV with variable time steps

Fulvio Scarano[1,*], Ilda Hysa[1,2], Adrian Grille Guerra[1], Marthijn Tuinstra[2], Andrea Sciacchitano[1]

1: Department of Aerospace Engineering, TU Delft, The Netherlands
2: Vertical Flight and Aeroacoustics Department, Dutch Aerospace Center
* Correspondent author: f.scarano@tudelft.nl

Keywords: particle tracking, trace detection, 3D, multi-exposure, directional ambiguity

ABSTRACT

Recording multiple exposures of the tracer particles onto a single digital image has the potential to simplify the hardware needed for 3D PTV measurements, especially when dealing with high-speed flows. Methods to devise the analysis of multiple-exposure recordings date back to the times when photography was the technique of choice, with the challenge of determining the time of each particle exposure. A sequence with equal time intervals leads to the well-known *directional ambiguity* problem. Instead, a sequence with irregular time-intervals (two or more) allows resolving the ambiguity. Two fundamental criteria are introduced that determine whether a set of particle samples corresponds to a physical trace for a given neighborhood: the kinematic similarity criterion imposes similarity (i.e. proportionality) between the length travelled by the particle and time elapsed. Additionally, the trace regularity criterion favors sets with minimum fluctuations of the velocity vector. A numerical algorithm, based on combinatorial analysis is presented, whereby all possible sets are scrutinized and the set of particles yielding the minimum disparity from the above criteria corresponds to the physical trace. False positives are eliminated on the basis of the signal-to-noise ratio defined in the space of all possible combinations. Such numerical implementation is challenged by the combinatorial growth of the calculations. The algorithm is demonstrated using 3D experimental data and results are benchmarked against the state-of-the-art time-resolved analysis *Shake-the-Box* (single-frame, single-exposure). Traces with three-pulses yield a detection rate of 85%. Detection declines with trace length. Conversely, the error rate (false trace) rapidly vanishes with the samples number, which confirms the reliability of trace detection criterion for a multi-pulse sequence. Furthermore, the limitations that need to be overcome before the technique can be applied in experiments are discussed.

1. Introduction

Three-dimensional velocity measurements are often needed in many flow regimes, such as vortex

dominated flows and turbulence in general. The last decade has witnessed a transition from the PIV measurement mode (high image density, cross-correlation motion analysis, double-frame recordings) towards the PTV mode (low image density, particle detection and pairing, multi-frame recordings). Numerous fundamental advantages are at the basis of such transition (see for instance the work from Kahler et al., 2012, and Cierpka and Kahler, 2012, among others), further supported by the advancement of scientific cameras (e.g. sCMOS imagers), highly scattering tracers (e.g. HFSB, Bosbach et al., 2009), safer and more versatile illumination devices (e.g. LED, Willert et al., 2010) and not least, more advanced algorithms for the particles motion analysis.
State-of-the-art three-dimensional particle tracking is based on the iterative 3D particle detection technique (IPR, Wieneke, 2012). Particle pairing, initially based on predictor-corrector techniques (Malik and Dracos, 1993) has been profoundly revised, resulting in a powerful and computationally efficient method (Shake the Box, Schanz et al. 2016).
Most of the current research focuses on single-pulse, double- or multiple-frame recordings the latter requires high-speed illumination and imaging. Comparatively, techniques based on multiple-exposure (ME) recordings have been mostly popular at the time of photographic PIV and rapidly declined with the advent of double-frame or kilohertz rate cameras (Hain et al. 2007). As a result, research on ME systems has appeared rarely in the literature in the last two decades.
The recent developments towards multi-camera redundant systems (Hysa et al., 2023; Hendriksen et al. 2024) foresee that 3D PTV systems will feature a multitude of imagers, well exceeding the typical set of three to four cameras, as used in tomographic PIV (Elsinga et al. 2006). Furthermore, performing the time-resolved analysis of aerodynamic flows in the range of 10 – 50 m/s requires increasingly high imaging rates and experiments are more commonly reverting to double-frame recording, to detriment of the velocity dynamic range and measurement reliability in general.
Recording multiple exposures on a single frame can potentially address the above trade-off, provided that the temporal information lost in the single-frame recording can be recovered. The analysis of ME recordings, however, has been and still remains a challenging problem, due to the loss of time-tag of the detected particles. For instance, Utami and Ueno (1984) performed the analysis of four-pulse recordings (Figure 1) with traces recognized by the user, including the assignment of the direction of motion. Early works dealt with planar illumination, mostly, and the problem of truncated traces by out-of-plane motion was approached by using a dot-streak-dot encoding of the particle image (Agüí and Jimenez, 1990). A solution to the problem of directional ambiguity was proposed by Grant and Liu (1990), with the pulse tagging technique, whereby the preceding and following pulses were differing in their intensity. Even though the research shifted its focus towards algorithms for the analysis of single-frame single exposure recordings, ME or streaks analysis maintain its research scope (Qureshi and Tien, 2022, among

others).

Streaks velocimetry, however, features high source density, and the condition of streaks overlap is rapidly reached. Furthermore, the streak intensity is inversely proportional to the local velocity, challenging streaks detection based on a single intensity threshold. Finally, also determining the streak length requires accurate detection of its origin and end. Methods to circumvent it have been proposed that use the dot-streak-dot pattern (Agui and Jimenez, 1991).

A specific development of the Shake-the-Box technique for double-exposure recordings has been proposed, whereby a total of four exposures are collected on a double-frame recording. The directional ambiguity is approached making use of either a tentative search or making use of a particle-space correlation to produce a statistical velocity predictor (Novara et al., 2019).

For a multiply exposed recording, the two main problems are the *time-tag* (i.e. establishing the correspondence of each dot to a time instant) and the *trace-tag* (i.e. associating multiple dots to the same physical tracer and defining its trajectory). The latter is also known for single-exposure systems as the *pairing* problem. When the density of particle images in the recording is increased, the distance between particle images becomes comparable to the distance travelled between pulses and the probability of false pairing grows exponentially, as discussed in the early works of Maas et al. (1993). Finally for 3D measurements, for a given concentration of the tracers, recording multiple positions of the particle tracers on a single image also increases the image density and the probability of ghost particles.

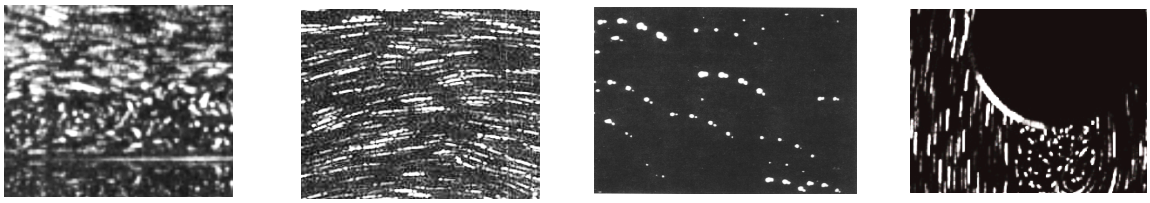

Figure 1 – Examples of ME recordings for PTV analysis of fluid flows. From left to right: four-pulse (repr. from Utami and Ueno, 1980); pulse-streak-pulse (repr. from Agui and Jimenez, 1990); Pulse-tagging (repr. from Grant and Liu, 1990); Streak velocimetry (repr. from Qureshi and Tien, 2022)

The present study examines the problem of *time-tag* and *trace-tag* assignment for multiply exposed recordings. The principle to resolve the directional ambiguity is that of sequence tagging, i.e. a specific pulse sequence is utilized, where the time intervals are irregular and do not exhibit time-symmetry. The result is an irregular sequence of dots, here called a *trace*, to be compared to the imposed sequence of illumination. The principle has been introduced in Hysa et al. (2022), who examined the impact of the sequence structure on the trace detectability. In the present study, a kinematic similarity criterion is introduced, which attempts recognizing simultaneously the trace as a sequence of dots along the particle trajectory (*trace-tag*) and resolves the directional ambiguity

of said dots (*time-tag*). The kinematic similarity criterion is combined with an additional constraint on the particle acceleration (*trace regularity*) whereby departure from similarity is penalized along with the L-2 norm of the acceleration along the trace. The two criteria yield a composite signal with the associated signal-to-noise ratio that is the backbone of the current method. The working principle is first illustrated with a numerical example and then demonstrated, using an experimental database of 3D measurements around a wall-mounted cube immersed in a turbulent boundary layer at Re = 80,000 based on cube height (Hendriksen et al. 2024).

2. Trace detection

When a tracer particle is illuminated by light pulses during its motion, it produces a pattern that depends upon its velocity and acceleration, the illumination sequence and the relative viewing direction. Once particle images are reconstructed in 3D space, the latter dependance is eliminated. Continuous illumination yields streaks, while regular pulses return mostly dotted straight or curved lines. Variations of the above have been illustrated in Figure 1, where most often, the sequence is obtained by equally spaced light pulses or a combination of dots and streaks. For a chosen time separation, the larger the number of pulses N, the higher is the measurement precision, as the velocity dynamic range is found to scale with $N^{3/2}$(Lynch and Scarano, 2013). Furthermore, a non-regular sequence has the potential to disambiguate the direction of motion. The principle, though intuitive, is schematically represented and clarified in Figure 2. A chosen sequence of illumination pulses (*temporal template*) with varying time separation translates into a sequence of dots (*marks*) in the image (*trace*) spaced by corresponding travelled paths. Let us define the particle trajectory Γ (Figure 2-left), with the sequence of N time instants corresponding to the light pulses $\tau = \{t_1, t_2, \ldots, t_N\}$, with $t_1 = 0$ and $t_N = T$. We indicate the normalized vector of time instants as $\tau^* = \tau / T$, such that $\tau^* \in [0, 1]$.

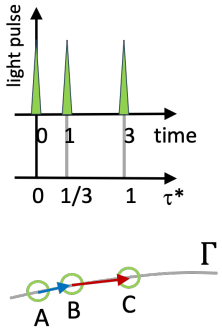

Permutation	Paths	$\varepsilon_{\sigma\tau}$	ε_{α}	$\Pi\varepsilon$
A – B – C		0.0	0.0	0.0
A – C – B		1.33	4.0	5.33
B – A – C		0.67	3.5	2.33
B – C – A		2.0	3.5	7.0
C – A – B		2.0	2.5	5.0
C – B – A		2.0	1.5	3.0

Figure 2 – left: three-pulse sequence temporal template and the corresponding trace (bottom). Right: time-tag permutation list and corresponding paths (blue for the first displacement and red for the second one). Output of *CKS*, *CKR* and composite detection criteria.

The particle position at such time instants is given as the vector of marks $\mathbf{X}_p = \{\mathbf{x}_1, \mathbf{x}_2, \ldots, \mathbf{x}_N\}$. Correspondingly, we indicate the travelled distance as $\sigma = \{s_1, s_2, \ldots, s_N\}$ with $s_1 = 0$. The normalized abscissa is $\sigma^* = \sigma / s_N$, resulting into $\sigma* \in [0, 1]$.

In the hypothesis that the variations of the particle tracer tangential velocity can be neglected along the trace, $\tau*$ and $\sigma*$ should obey the *criterion of kinematic similarity* (*CKS*), i.e.:

$$\varepsilon_{\sigma\tau} = \{\sum_{i=1}^{N}[(\sigma_i^* - \tau_i^*)^2]\}^{1/2} = 0. \qquad (1)$$

Such criterion needs to be evaluated for all possible choices of the time-tag, which corresponds to the $N!$ permutation of their index. The situation is illustrated in Figure 2-right, where the order of the time-tags (A-B-C) is varied according to the permutations, each corresponding to a possible path. The latter is inspected by eq. 1, yielding the residual e_{st}. For this given set of N particle marks, a trace of rank N ($\Im_N$) can be detected based on the criterion that selects the case (viz. permutation) with minimum disparity between the temporal template and the normalized path:

$$\min_{\Im}\{\varepsilon_{\sigma\tau}\}_K, \qquad (2)$$

Where K is the number of possible permutations from the N considered particle images ($K = N!$). The evaluation of such criterion is illustrated in the first column on the right of Figure 2 for the case $N = 3$. An additional criterion, frequently adopted in PTV analysis is based on the piecewise estimation of the acceleration of the particle. The *criterion of kinematic regularity* (*CKR*) reads as

$$\min_{\Im}\{\varepsilon_{\alpha}\}_K, \qquad (3)$$

Where ε_α is defined as the sum of the standard deviation from each component of the velocity vector along the piecewise trajectory. An example for this criterion is also given in Figure 2 for the simplified case of a trajectory with negligible Lagrangian acceleration.

The above criteria are imposed simultaneously and combined through their product $\prod \varepsilon = \varepsilon_{\sigma\tau} \times \varepsilon_\alpha$; the latter yields a composite signal defined in the space of particle time-tag permutations. Correspondingly, a *composite detection criterion* (*CDC*) is defined as follows:

$$\min_{\Im}\{\prod \varepsilon\}, \qquad (4)$$

The last column in Figure 2 shows this quantity and indicates how the combination of these two criteria improves the trace detectability, identifying the correct permutation of time-tag as that exhibiting the furthest distance between the absolute minimum and the second lowest value. Based on the latter quantities a signal-to-noise ratio can be introduced in the space of the

permutation index as the ratio between absolute minimum and the second lowest value of the composite detection criterion. In this example, the second lowest value is 0.67, 1.5 and 2.33 for e_{st}, e_a and Pe respectively.

The value corresponding to the correct sequence in this example is zero, given the ideal conditions considered (no noise and zero acceleration). In realistic condition, an estimate of such minimum is typically $o(0.1)$, when considering the combined effect of measurement and trajectory modelling uncertainties altogether not exceeding 10%. When the two criteria are multiplied, the composite criterion is expected to yield a minimum in the order of 10^{-2}. Instead, the spurious permutations yield values remaining in the order 1 or larger. As a result, the signal-to-noise ratio of the composite criterion is expected in the order of 100 or above, which indicates a favorable condition in terms of trace detectability.

2.1 Numerical example

With the purpose to illustrate the principle of the algorithm a simplified numerical example is presented here, where a set of particle images belongs from one complete trace and two additional marks spurious to the trace. Figure 3 illustrates two conditions: on the left, the spurious marks lie at distance from the trace, whereas on the right, they appear along the trace and may be confused with it.

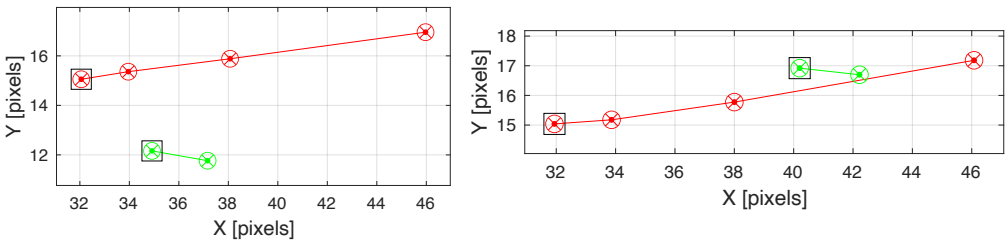

Figure 3 – A set of 6 candidate particle samples, of which 4 pertain to a trace (red labels) and 2 are from an incomplete, truncated, trace. Left: distance between spurious particle images and trace is larger than particle displacement. Right: distance is smaller than displacement.

The detection criteria are evaluated numerically and the result is shown in Figure 4. The top row displays the evaluation of the red trace on the left of Figure 3: 1) the residual of particle position as expected from the kinematic similarity; 2) the residual from the piecewise acceleration; 3) the composite criterion.

In this case, the four marks composing the trace are correctly selected, given that the spurious marks are sufficiently apart. The criteria are evaluated for all 24 permutations (4!) of such four

marks. It can be observed that the minimum for *CKS* is in the order of 10^{-2} and that of *CKR* in the order of 10^{-1}. The composite criterion yields therefore a minimum in the order of 10^{-3}, which compared to the second lowest value of unit order of magnitude yields a signal-to-noise ratio *SNR* in the range of 10^{3}.

The situation on the right of Figure 3 features the spurious marks (green) in close proximity of the main trace (in red). In this case, the four marks selected for the analysis contain one spurious mark and the results are shown in the bottom row of Figure 4. Both *CKS* and *CKR* exhibit a minimum in the unit order of magnitude. As a consequence, also the composite criterion returns a minimum of unit order, not significantly separated from the second lowest value. The low level of the *SNR* ($SNR_{CDC} < 2$) allows to conclude that the selected set of marks does not belong to the same particle and the trace is not accepted as a valid measurement.

In the latter example, the importance of preselecting the sets of marks that candidate to form a trace is emphasized. From combinatorial analysis, the number of possible permutations of M marks by groups of N is given by:

$$P = \binom{M}{N} = \frac{M!}{(M-N)!N!} \tag{5}$$

It should be retained in mind that the value of P increases very rapidly with M. Thus, any algorithm using this approach requires a careful choice of the minimum neighborhood for trace evaluation. In absence of additional criteria that limit the selection of the samples, it is therefore necessary that the number of marks considered to identify a trace are taken in relatively small subgroups by preselection (e.g. $M < 10$ and $N < 5$). For every candidate trace, the detectability criteria need to be evaluated for every permutation of the time-tag, with a total of $K = N!$ possibilities as illustrated in Figure 2, where $N = 3$ and $K = 6$. Combining both requirements returns a total number of evaluations, Q, that scales as:

$$Q = P\,N! = \frac{M!}{(M-N)!N!}\,N! = \frac{M!}{(M-N)!} \tag{6}$$

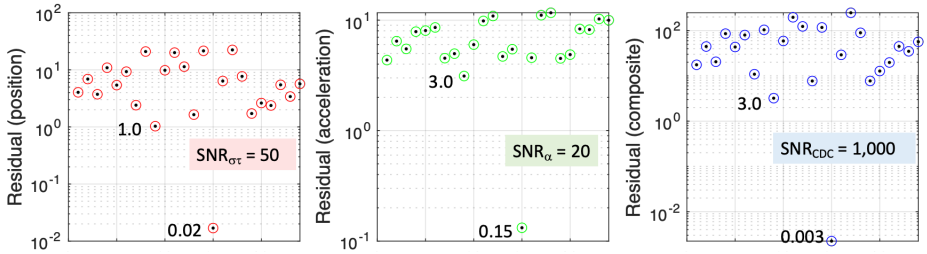

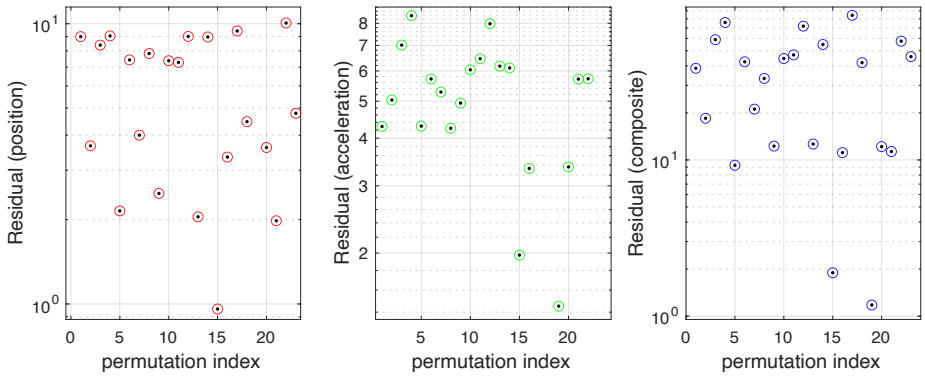

Figure 4 – Values of the position residual $\varepsilon_{\sigma\tau}$ (left, criterion of kinematic similarity), acceleration residual ε_{α} (middle, criterion of kinematic regularity) and their product (right) as a function of particle permutation within a set. Top row corresponds to Figure 3-left, where all selected marks belong to a physical trace. Values of first and second minimum are indicated, that lead to the *SNR*. The bottom row corresponds to Figure 3-right, where a spurious mark is included in the quartet, as spurious marks occur in vicinity of the trace.

Due to the computational burden associated to the proposed method, approaches that reduce the complexity of both the candidate trace selection and time-tag permutation have been explored and their effect on the computational time required are discussed in section 6.

3. Numerical algorithm

The above principles are implemented in a numerical algorithm, schematically depicted in Figure 5. The process considers as input the recording of multiply exposed images of particles (box *a*) such as illustrated in Figure 7-right. Particle image triangulation (e.g. IPR, box *b*) yields 3D particle positions, however at unknown time instants (box *c*), of which an example is illustrated in Figure 8. The algorithm interrogates particle exposures selecting them one by one (box *d*). A search region is chosen around the exposure (box *e*), based either on the maximum expected velocity or a local estimate of the velocity, when available (Figure 9-right), and the total time elapsed between the first and the last pulse. The minimum search diameter d_s must include the entire trace, which turns into the condition that $d_s \geq V \cdot T$. In this case, when marks at the edge of trace are selected, the search region does not include the whole trace and the search fails. When a mark in the middle of the trace is considered, the search region includes the whole trace, which may be detected if it obeys the composite detection criterion. This is schematically illustrated in Figure 9-right.

Assuming that M marks fall within the search region (box *f*) around the selected mark, the combinations with N-1 candidate marks is considered (each group of N marks includes the

selected mark). All combinations of M-1 marks by groups of N-1 are considered (box g).

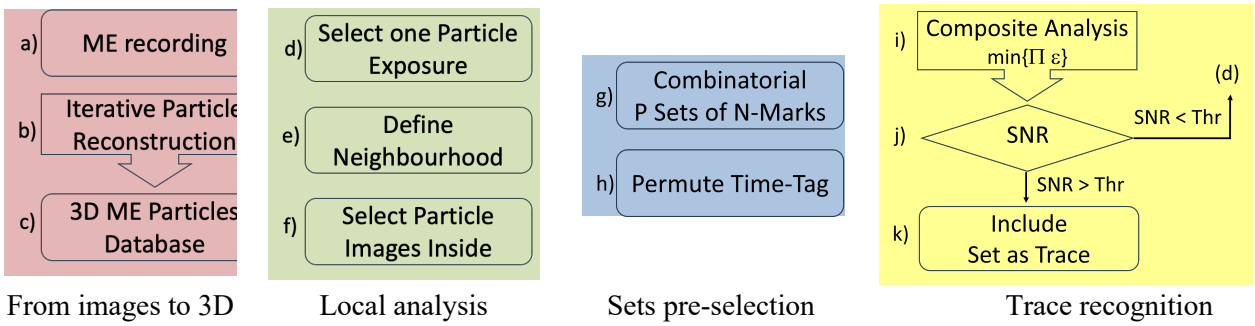

Figure 5 – Flow chart describing the main operations of the *trace* algorithm. Main blocks highlighted in the lower row.

For each combination, all possible time-tag permutations are considered (box h, see also Figure 2-right), over which the *CDC* from eq. 5 is applied (box i). The value of the *SNR* (such as in Figure 4) with respect to a chosen threshold value (box j) determines accepting the set as a trace (box k) or discarding it and move back (to box d). The process terminates when all particle exposures have been considered or assigned.

4. Experimental database

Experiments are conducted in the W-tunnel, a low-speed open jet facility at the aerodynamics laboratories of the Aerospace Engineering Department of TU Delft. A cube of side-length 12 cm is installed on a flat plate immersed in a stream at 10 m/s. A turbulent boundary layer develops on the plate with approximately 2 cm thickness. The cube height-based Reynolds number is Re = 80,000. The flow is seeded with helium filled soap bubbles (HFSB, neutrally buoyant, 300 mm median diameter) released by a 200-generator seeding rake integrated in the wind tunnel (Jux et al. 2020). The tracers' concentration is approximately 1 bubble/cm^3. The layout of illumination and imaging systems is shown in Figure 6: two *LED-Flashlight 300* arrays from LaVision produce pulsed illumination at a rate of 3 kHz. Seven high speed CMOS cameras (Photron *FastCam SA-1*, 1 Mpx, 5,400 fps, 12 bits) capture the light scattered by the HFSB tracers. The 7 cameras are distributed with their view such to cover the entire object and the flow field around it, to study accurate object position registration (Hendriksen et al., 2024) and its integration within the 3D particle tracking measurement (Wieneke and Rockstroh, 2024). In the present study, a thin section of data is considered for sake of conciseness. The data domain encompasses the (X,Y,Z) range ([–

15, 20], [–2,2], [–12, 12]) cm^3 respectively. Although the measurements are conducted at a constant rate of 3kHz, irregular time separation is simulated by skipping frames in the analysis. Ground-truth data is obtained making use of the Lagrangian Particle Tracking *Shake-the-Box* algorithm (available in the LaVision DaVis 10 software) for the full time-resolved sequence.

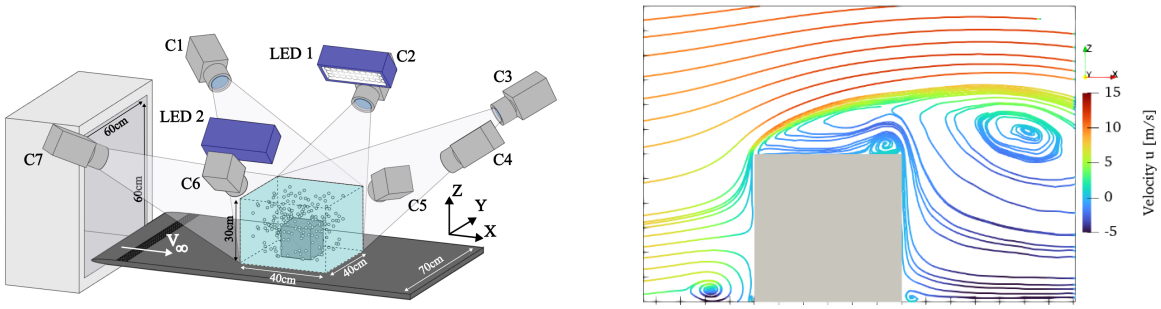

Figure 6 – Left: experimental arrangement and layout of the 3D particle tracking system. Right: time average, velocity color-coded, streamlines pattern in the median plane. (tick marks spaced by 2 cm).

By recording particle images during ME, the imaged density of particle images increases significantly. This aspect poses limitations to the maximum spatial concentration of the tracers and is discussed in the remainder. Figure 8 illustrates the above by comparing particle image recordings in the regimes of single (left) and four (right) exposures in sequence of pulses at □ = {0, 0.33, 1.0, 2.0} ms. The latter is obtained as the sum of intensity from the single exposure images. In the present work, the analysis is performed simulating the ME recordings and analyzing directly the reconstructed 3D position of particles. Figure 8 presents the 3D particle tracers positions for the case of double- and ME with uniform time separation, which is chosen to illustrate the problem of directional ambiguity arising from double exposure or ME with regular time intervals.

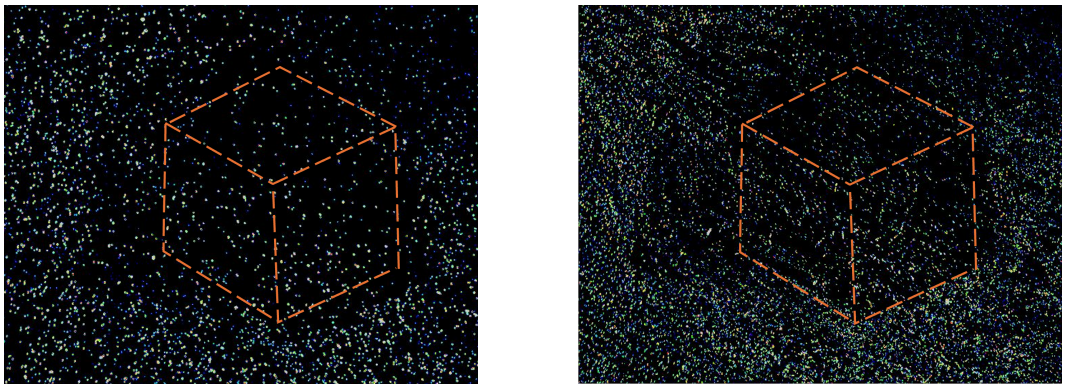

Figure 7 – Images of HFSB tracers from a single (left) and triple exposure recorded from one of the seven cameras. Exposures at τ = {0, 0.33, 1} ms. Object position outlined with orange dashed edges.

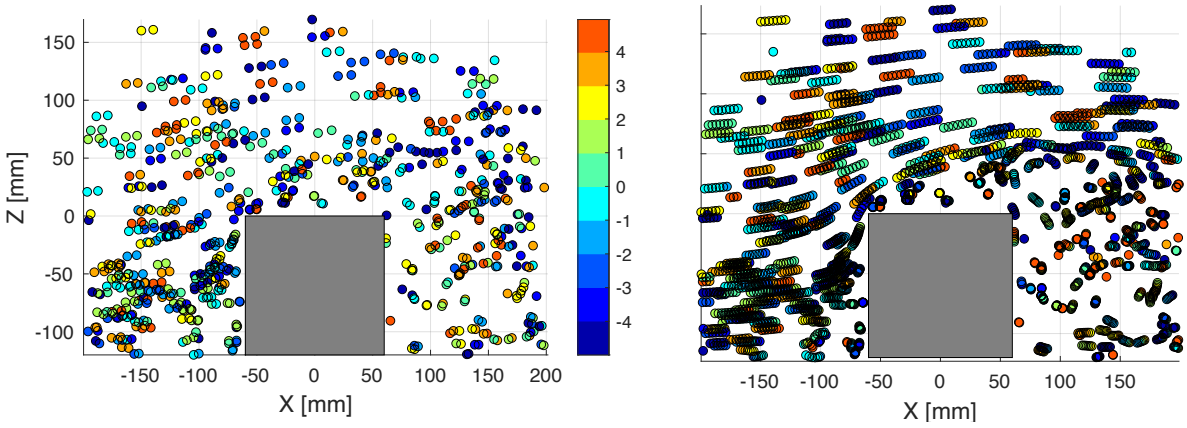

Figure 8 – 3D particles positions from the experimental database. Color coded depth position (in mm). Left two time instants ($N = 2$) separated with 1 ms. Right: six time instants ($N = 6$) with 0.33 ms uniform time separation.

5. Results

In Figure 9 the example of a four-pulse single-frame recording is shown, according to the time instants sequence $\tau = \{0, 0.33, 1.0, 2.0\}$ ms. An enlarged view (Figure 9-right) of a region of the flow allows to appreciate the particle positions and their arrangement into traces that resemble the template imposed by the pulse sequence. The illustration shows the example of a few particles taken for the neighborhood analysis. Clearly a spherical search region conservatively admits a larger number of particles in the set for the analysis. The minimum radius can be put to half of the expected travelled distance. As a result, only when the particle sample in the middle of the trace is interrogated the trace can be fully comprised and detected (green shaded circle). Instead, when particle samples at the edge of the trace are considered, the search will fail (red shaded circle). It can be easily seen that a-priori knowledge of the local velocity significantly reduces the search volume and the corresponding number of particle samples included in the analysis (green shaded rectangle).

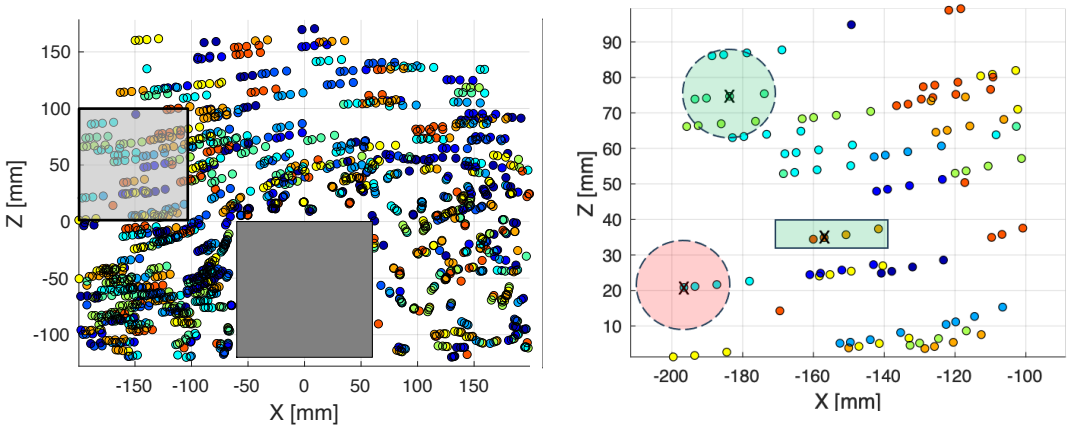

Figure 9 – Particles positions from the experimental database. Color coded depth position (in mm). Left: 4-exposure recording with irregular (increasing) time separation. Right: zoomed view from the shaded square in the left picture. Isotropic (circles) and adapted (rectangle) neighborhoods are shown. The green color indicates that all exposures from the trace are captured. The red color indicates incomplete set of exposures.

An illustration of the detection process is given in Figure 10, where particles are displayed along the velocity vector (top-left), as obtained from the time-resolved analysis of STB. The velocity vector information, however, is not used in the detection process here. When the particle samples at the edge of the trace are considered, the search region does not include the entire trace and most detections fail (top-right). For samples inside the trace, depending on the local velocity, some sets return a correct trace or a spurious one (bottom-left). Finally, the particle samples close to the trace mid-point mostly include the full set of samples comprised in the trace and return a correct measurement (bottom-right).

When the number of pulses N is increased, the probability of erroneously detection further decreases as a result of the increased uniqueness of the sequence. This aspect can be regarded as the analogous of increasing the number of particle tracers in the correlation window for PIV analysis, which is known to increase the signal-to-noise ratio of correlation. However, adding more pulses to the sequence has two important shortcomings: 1) the overall number of particle images in the recording increases and the probability of ghost particles with it; 2) adding pulses and increasing the total time of the sequence increases exponentially the computational burden associated with a large search region for the trace.

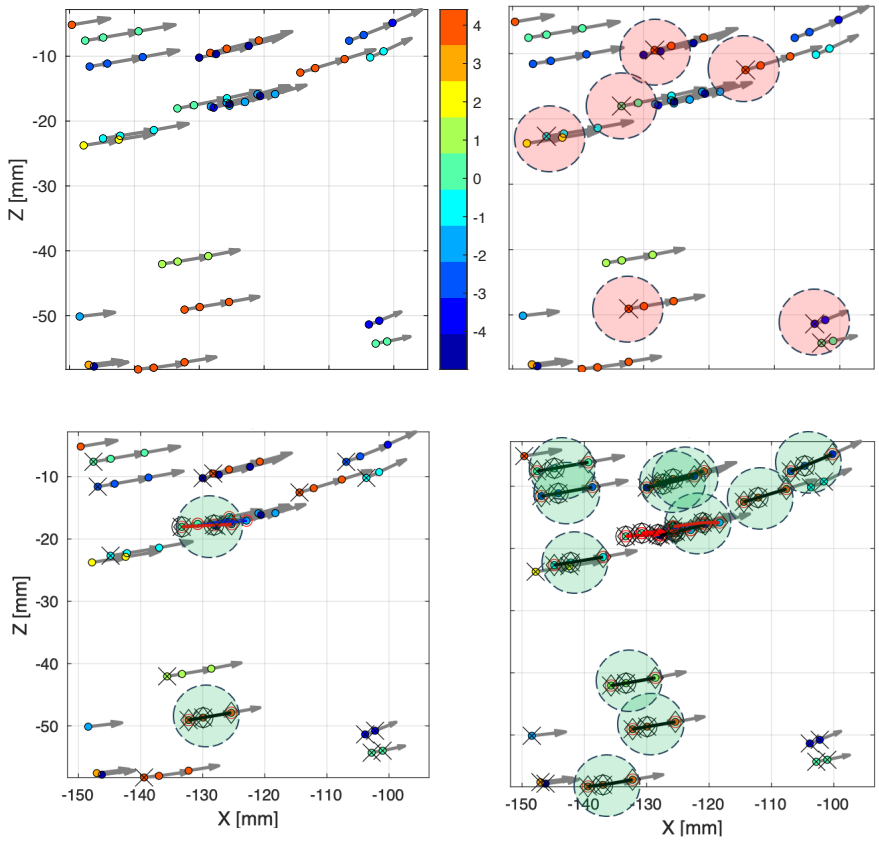

Figure 10 – Particle selection and trace detection in a sample region. Top-left: particles and velocity vectors from the STB analysis. Top-right: selected particles (denoted by a black cross) that do not lead to a trace because their neighborhood does not include enough samples. Bottom-left: when a particle's neighborhood contains sufficient samples, the set is subject to the composite detection criterion. Two traces are detected (around the large-circled particle), of which one is erroneous (in red). Bottom-right: the process advances for all the particles. Most errors occur in regions of nearly overlapping traces.

The number of pulses is varied from 3 to 6 adopting a simple rule for the time separation, which increases linearly between pulses. This is realized by skipping frames from the time-resolved sequence. The case with $N = 3$ considers frames 0, 1 and 3. Furthermore for $N = 4$, frames 0, 1, 3 and 6 are considered. The longest sequence ($N = 6$) has been taken with a different rule for the time separation, which avoids the excessive length of the trace and at the same time gives an indication of the effect of N maintaining the same travelled path as for the case $N = 5$.

The corresponding pulse time and their separation are given in the first rows of table 1. The original single-exposure recordings feature approximately a density of particle images of 0.02 particles-per-pixel (ppp). Therefore, the density of particle images for the ME recordings is obtained multiplying the single-exposure value by the number of exposures N. The detection criterion (box *j* in

Figure 5) has been set conservatively at SNR > 100. Furthermore, varying this threshold in the

range 30 to 300 has shown not to bring considerable differences in the results.
The number of detected particles increases linearly with *N*, but the number of STB traces remains approximately constant. The same occurs for the number of detected traces. The relative detection rate is defined as the number of detected traces compared to the traces obtained with time-resolved single frame analysis performed with the STB algorithm.
The results indicate that for the minimum trace, composed of three samples, a relatively high rate of detection is obtained (81 %), with the number of spurious detections amounting to 5.6 %. Increasing the number of pulses to 4 reduces the detection rate. However, the additional pulse yields a significant benefit in terms of reliability, with the error rate dropping below 1%. Further increases in the exposures involve more computations. Yet, the detection rate declines further, to a minimum in the range explored here, of 60% for $N = 6$, and a negligible error rate (0.1%). The latter effect is ascribed to the hypotheses of constant velocity, at the basis of the detection criterion. Dynamic thresholding and/or multi-pass interrogation are expected to possibly solve for this effect. Their implementation and validity, however, go beyond the scope of this study and are not included here, for conciseness.

Table 1 – Settings of ME recording and summary of results from the experimental database.

N	**3**	**4**	**5**	**6**
Frame index I_F **ΔI_F**	0 – 1 – 3 1 – 2	0 – 1 – 3 – 6 1 – 2 – 3	0 – 1 – 3 – 6 – 10 1 – 2 – 3 – 4	0 – 1 – 3 – 6 – 7 – 10 1 – 2 – 3 – 1 – 3
Time [ms]	0 – 0.33 – 1.0	0 – 0.33 – 1.0 – 2.0	0 – 0.33 – 1.0 – 2.0 – 3.3	0 – 0.33 – 1.0 – 2.0 – 2.33 – 3.3
[i]ppp	0.06	0.08	0.1	0.12
[ii]N_p **N_{tracks} (TR-STB)**	4147 1370	5233 1358	6814 1363	8176 1362
N_{tracks} (ME-PTV)	1144	926	861	826
Detection rate	81 %	68 %	63 %	60%
[iii]Erroneous	62	27	2	1
Error rate	5.6 %	2.9 %	0.3 %	0.1 %

[i] Based on estimated ppp = 0.02 from single exposure (Hendriksen et al. 2024)
[ii] Number of detected particle exposures, based on TR-STB
[iii] Criterion for erroneous trace $Err_U > 0.3\ V_\infty$

6 Algorithm accelerators

One of the challenges of the proposed methodology is the computational burden associated to the combinatorial nature of it. The requirements quickly increase when considering more exposures

due to the associated larger neighborhood search radius, the number of trace candidates (eq. 6) and time-tag permutations. A powerful way of relaxing the computational requirements is the use of a velocity predictor to adapt the search region around a particle, as sketched in Figure 9-right by employing a rectangular shape instead of an isotropic search radius. The use of a predictor could come from an iterative implementation of the method, or within a spatial dilation of the measured domain. Both methods are subject to further research.

6.1 Linear-fit pre-selector

Besides the use of a predictor, two different strategies have been explored to reduce the cost of the candidate trace selection (box *g* in Figure 5) and time-tag permutation (box *h*) respectively. The first approach consists of preselecting a particle trace based on their straight alignment, evaluated with a least squares linear fit (*linear fit pre-selector*). Assuming that *M* marks fall within the search region around the selected mark, the combinations with *N*-1 candidate marks are considered (each group of *N* marks includes the selected mark). The set with the lowest residual is considered as candidate trace and undergoes the time-tag permutation analysis. This simplifies the evaluations of the detectability criteria from *Q* possibilities (eq. 7) to *P* evaluations (eq. 6) of the linear fit followed by *N* ! time-tag permutations. The approach is illustrated in Figure 11 for a three-pulse sequence.

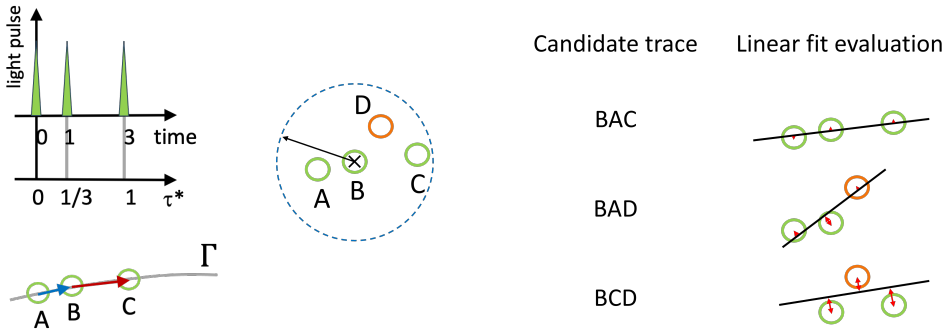

Figure 11 – left: three-pulse sequence temporal template and the corresponding trace (bottom). Middle: search region and neighborhood around the selected mark. Right: linear fit evaluation of all trace possibilities, with the residuals shown in red.

6.2 Direction disambiguation

Once a candidate trace has been selected, the time-tag permutation analysis (blok *h*) can be simplified by restricting the search to only those combinations where the velocity direction between subsequent illuminations does not vary beyond 90 degrees. The latter, is considered a conservative criterion, considering that for most cases, a spurious time-tag permutation results in almost complete reversal of some displacements along the trace. The operation is computationally efficient considering that the trajectory has been approximated as rectilinear and the criterion is coded as sign reversal detection (dot product of subsequent displacement vectors, Figure 12). The result yields only two possible permutations (instead of $N!$). The two candidates are then inquired with the composite detection criterion, as illustrated in the last column of Figure 12, for a three-pulse sequence.

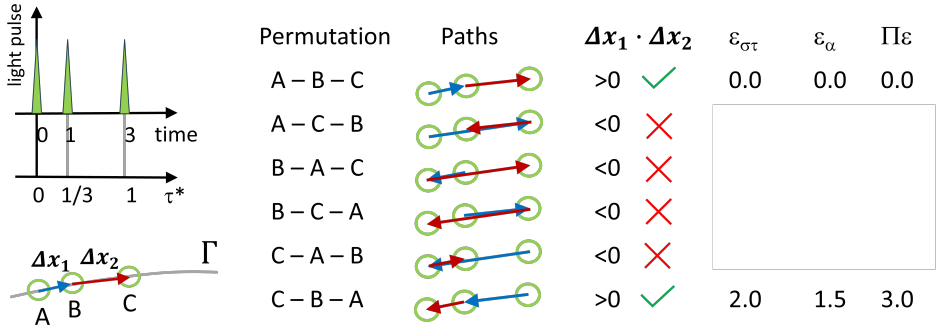

Figure 12 – Left: three-pulse sequence temporal template and the corresponding trace (bottom), together with the displacement vector $\Delta\mathbf{x}_1$ and $\mathbf{\Delta x_2}$. Right: time-tag permutation list, corresponding paths (blue for the first displacement and red for the second one), direction disambiguation and output of the detectability criteria for the appropriate permutations.

6.3 Computational effort

The effect of the proposed accelerators in the computational effort of the ME evaluation algorithm is summarized in table 2, by comparing the CPU time required to evaluate the recordings presented in table 1. The analysis compares the most expensive analysis, that makes no use of the above accelerators, the linear fit pre-selector and the linear fit followed by the direction disambiguation. All computations have been performed in a workstation equipped with an Intel Xeon W-2223 CPU.

Table 2 – CPU time required for the evaluation of the ME algorithm for the experimental database.

N	3	4	5	6
CDC (no accelerators)	0.3 s	3 s	14 h	>1 day
Linear fit pre-selector	0.3 s	1 s	1 min	15 min
Linear fit + directional detector	0.2 s	0.5 s	20 s	3 min

The results indicate an explosive computational burden with trace length/rank when for the evaluation makes no use of accelerators. The linear-fit pre-selector provides already a strong reduction of the number of combinations, resulting in a substantial reduction of the computational effort the longer traces. Finally, the one-directional time-tag brings a modest reduction of computational effort, yet appreciable for the longer sequences. It must be noted that the additional restrictions posed by the accelerators (straight trajectory, no direction reversal) may not hold true in highly turbulent regions, where the tracers follow highly curved trajectories. This may increase the occurrence of false negatives (missed detections) of such trajectories. Still, the accelerators represent a powerful tool to produce a first estimate of the velocity field, for use as a predictor in an iterative algorithm.

7 Application potential and bottlenecks of ME PTV

Several aspects deserve attention for the further pursuit of this technique. The main positive points are that the use of traces from ME recordings significantly lowers hardware requirements: the ME-PTV does not require high-speed imagers, neither short interframe separation time. It is therefore expected that experiments can be conducted using ordinary single-frame monochrome cameras.

A second positive aspect is the reduction of data storage, as the velocity measurement is based on a single image. Furthermore, the free choice of the number of exposures allows to tune the image density.

Finally, when compared with double-frame single-exposure, traces of 3 or more exposures offer a higher measurement dynamic range (Novara et al., 2023), which compares to state of the art techniques based on time-resolved single-exposure recordings (e.g. STB).

Among the most problematic aspects of this technique are the regions with low to zero velocity, where samples of the particle image will overlap and will not yield a distinct entry for the particle position. The current technique fails to detect traces in such conditions and additional criteria will be needed for the treatment of low-velocity conditions. A second point of attention is the limit of

seeding concentration: the ME recording multiplies the number of particle images in a single recording and as such, it aggravates the problem of ghost particles formation. This aspect can be mitigated with the use of a multitude of cameras (e.g. $N_{cam} > 10$), currently not practiced in conventional 3D PIV experiments due to costs and complexity.

8 Conclusions

A novel measurement approach (ME-PTV) is proposed, to analyze the 3D motion of particle tracers, based on multi-exposed recordings. The specific choice of irregular timing of illumination produces *traces* from particle images, with a specific pattern, easier to recognize and at the same time, solving the problem of the unknown *time-tag*. The detection of a trace is based on kinematic similarity, reinforced with a kinematic regularity criterion that penalizes particle acceleration. All together these two criteria allow identifying traces from clusters of measured particle positions. The method requires the definition of a detection criterion, based on the SNR of the composite signal. The application to experimental data shows a maximum detection rate above 80% when $N = 3$, declining to approximately 60% for $N = 6$. Correspondingly, the error rate attains 6% and 0.1% for the above choices. More than 90% of the detected traces exhibit a SNR larger than 100, indicating the robustness of the trace detection algorithm.
The sequence length is limited by the upper limits on image density and the occurrence of ghost particles. Furthermore, long traces involve an increasing computational effort due to the combinatorial nature of the search and detection algorithm. Based on the current study traces with 3 to 4 pulses are sufficient to guarantee a high detection rate error rate in the order of 1%. The lower limit of measurable velocity, due to the effect of overlapping particle images, is left out to the scope of the present work and will be the subject of further research.

Acknowledgements

The experimental database has been made available by Luuk Hendriksen, who is kindly acknowledged.

References

Adrian, R.J., & Westerweel, J. (2011). *Particle image velocimetry*, Cambridge University Press, Cambridge, UK.

Agüí, J.C., & Jimenez J. (1987). On the performance of particle tracking, *Journal of Fluid Mechanics*, 185.

Bosbach, J., Kühn, M., & Wagner, K. (2009). Large scale particle image velocimetry with helium filled soap bubbles, *Experiments in Fluids*, 46, 539–547.

Cierpka, C., & Kähler, C.J. (2012). Cross-correlation or tracking—comparison and discussion. In: *16th Int. Symp. on Applications of Laser Techniques to Fluid Mechanics, Lisbon, Portugal.*

Grant, I., & Liu, A. (1990). Directional ambiguity resolution in particle image velocimetry by pulse tagging, *Experiments in Fluids*, 10, 71-76.

Hendriksen, L.A., Sciacchitano, A., & Scarano, F. (2024). Object registration techniques for 3D-PIV/LPT. In: *21st Int. Symp. on Applications of Laser and Imaging Techniques to Fluid Mechanics, Lisbon, Portugal.*

Hain, R., Kähler, C.J., & Tropea, C. (2007). Comparison of CCD, CMOS and intensified cameras, *Experiments in Fluids*, 42, 403-411.

Hysa, I., Scarano, F., Sciacchitano, A., & Tuinstra, M. (2022). Time-space correlation of multiple-exposure PTV with incommensurable intervals. In: *20th Int. Symp. on Applications of Laser and Imaging Techniques to Fluid Mechanics, Lisbon, Portugal.*

Hysa, I., Scarano, F., Sciacchitano, A., & Tuinstra, M. (2023). A multi-directional redundant 3D-PIV system for ship deck wind interactions. In: *15th International Symposium on Particle Image Velocimetry – ISPIV, San Diego, USA.*

Jux, C., Sciacchitano, A., & Scarano, F. (2020) Flow pressure evaluation on generic surfaces by robotic volumetric PTV, *Measurement Science and Technology*, 31, 104001.

Kähler, C.J., Scharnowski, S., & Cierpka, C. (2012) On the uncertainty of digital PIV and PTV near walls, *Experiments in Fluids*, 52, 1641-1656.

Kähler, C.J., Scharnowski, S., & Cierpka, C. (2012) On the resolution limit of digital particle image velocimetry, *Experiments in Fluids*, 52, 1629-1639.

Lynch, K., & Scarano, F. (2013) A high-order time-accurate interrogation method for time-resolved PIV, *Measurement Science and Technology*, 24, 035305.

Maas, H.G., Gruen, A., & Papantoniou, D. (1993) Particle tracking velocimetry in three-dimensional flows, Part 1. Photogrammetric determination of particle coordinates, *Experiments in Fluids*, 15, 133–146.

Malik, N.A., & Dracos, T.H. (1993) Lagrangian PTV in 3D Flows, *Applied Scientific Research*, 51,

161-166.

Novara, M., Schanz, D., Geisler, R., Gesemann, S., Voss, C., & Schröder, A. (2019) Multi-exposed recordings for 3D Lagrangian particle tracking with multi-pulse Shake-The-Box, *Experiments in Fluids*, 60, 1-19.

Novara, M., Schanz, D., & Schröder, A. (2023) Two-Pulse 3D particle tracking with Shake-The-Box, *Experiments in Fluids*, 64, 93.

Qureshi, M.H., & Tien, W-H. (2022) Novel streak-resolving algorithm for particle streak velocimetry, *Flow Measurement and Instrumentation*, 87, 102208.

Raffel, M., Willert, C.E., Scarano, F., Kähler, C.J., Wereley, S.T., & Kompenhans, J. (2018) *Particle Image Velocimetry - A Practical Guide*. Springer-Verlag, Heidelberg, DE

Schanz, D., Gesemann, S., & Schröder, A. (2016) Shake the box: Lagrangian particle tracking at high particle image densities. *Experiments in Fluids*, 57, 1–27.

Utami, T., & Ueno, T. (1984) Visualization and picture processing of turbulent flow, *Experiments in Fluids*, 2, 25–32.

Wieneke, B. (2012) Iterative reconstruction of volumetric particle distribution, *Measurement Science and Technology*, 24, 024008.

Wieneke, B., & Rockstroh, T. (2024) Lagrangian particle tracking in the presence of obstructing objects, *Measurement Science and Technology*, 35, 055303.

Willert, C., Stasicki, B., Klinner, J., & Moessner, S. (2010) Pulsed operation of high-power light emitting diodes for imaging flow velocimetry, *Measurement Science and Technology*, 21, 075402.